Aerodynamic characterisation of an experimental tilt-wing aircraft

Alexander Grima*

KTH Royal Institute of Technology, SE-100 44 Stockholm, Sweden

Computational analysis of experimental aircraft prior to test flights can be a valuable tool to estimate flight characteristics and determine areas of elevated caution. It can also provide feedback to software and model developers as to the accuracy of models used when the aircraft is ultimately flown. This paper describes the aerodynamic analysis and characterisation of an experimental tilt-wing aircraft with a unique design. The paper covers what analysis is performed as well as results of these aircraft characterisations. Through this analysis a database file is created for use with NASA Design and Analysis of Rotorcraft (NDARC) tool.

Nomenclature

C_{D0}	Zero lift drag coefficient,
C_D	Drag coefficient,
C_L	Lift coefficient,
C_M	Pitching moment coefficient,
F_x	Force in x-axis(Drag), N
F_z	Force in z-axis(Lift), N
M_x	Moment in x-axis(Roll), Nm
M_y	Moment in y-axis(Pitch), Nm
M_z	Moment in z-axis(Yaw), Nm
t	Time interval, s
l_{test}	Length of test length for time interval t, m
ψ	Ratio of particle movement and cell size,
RPM	Revolutions per minute, min^{-1}
$V_{forward}$	Forward(freestream) velocity, m/s
R	Radius of rotor, m
T	Thrust, N
A	Disk area, m^2
ρ	Air density, kg/m^3

I. Introduction

This paper investigates the aerodynamic characteristics of the Elytron 2S experimental tilt-wing aircraft.[1] This analysis is performed with the computational tools Athena Vortex Lattice (AVL),[2] XFOIL,[3] and RotorcraftCFD (RotCFD).[4] The analysis is done for the aircraft in hover and forward flight; an analysis of the aircraft's unorthodox hover control is also performed.

With the aerodynamic data calculated through the above analyses a database for the NASA Design and Analysis of Rotorcraft (NDARC)[9] tool is constructed to allow trim and flight dynamic analysis to be performed.

Initially the AVL analysis is covered to then lead into a RotCFD analysis performed for comparison to AVL. With these results compared, a RotCFD analysis is performed of the aircraft in forward flight and in hover. The analysis terminates in that of the louver control system to then culminate in a brief description of the NDARC database and conclusions drawn through the work performed.

A. Elytron 2S

The Elytron 2S is a single seater prototype for an advanced VTOL concept aircraft weighing $900kg$ consisting of a box wing and a small centrally mounted tilt-wing with rotors. The concept aircraft is proposed in two sizes, 4 and 10 seaters, and is envisaged for use as an air taxi, or perhaps for transportation of crews of oil and gas rigs.

This aircraft utilises a unique control system in hover; the design deflects the rotor wake with louvers, in comparison to conventional helicopter controls, i.e. swashplate, collective, and cyclic. As shown in *Figure 1*, these louvers are centrally mounted under the rotors to allow control of rate of climb, roll, and yaw. Pitch control is achieved by using a rear mounted air blowing system.

As the design of the rotors for the aircraft is not yet complete, rotor models developed for the XV-15[17] have been taken and scaled to the application of this aircraft. Due to the implementation of louvers it is

*M.Sc. Student, Aerospace engineering, KTH Royal Institute of Technology.

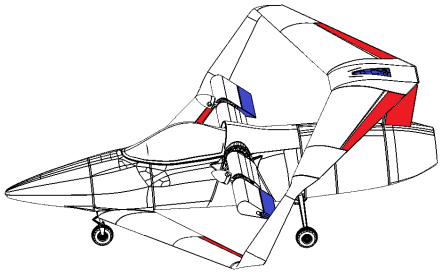

Figure 1: Control surfaces of the Elytron 2S experimental tilt-wing aircraft; blue highlighting control in hover mode and red control in aircraft mode.

not expected that collective will be required, therefore the collective of the rotor model is fixed at a value that will generate the expected thrust in hover. In forward flight the rotor speeds are reduced to bring down the tip speed.

B. AVL

AVL is used for the initial characterization of aerodynamic effects. This software uses an extended vortex lattice model for lifting surfaces and a slender-body model for fuselages and nacelles, makeing it suitable for analysis of rigid aircraft of an arbitrary configuration.[2] With AVL it is possible to make estimations of aerodynamic characteristics of each lifting surface individually; something that is required to build the NDARC database. The validity of AVL is explored by Pereira[18] showing AVL lift results comparable to wind tunnel data.

C. RotCFD

RotorcraftCFD is a recently developed mid-fidelity CFD tool designed specifically for rotorcraft analysis.[13,14] It is possible to model rotors both with an actuator disk model and with a blade element model. This is done with two-dimensional aerofoil data allowing for relatively fast computations in unsteady cases. Recently, RotCFD has been released in a parallesied version allowing for even faster analysis of rotorcraft. This software has been used extensively within NASA Ames Research Center's Aeromechanics branch to analyse rotor models,[15] as well as wind tunnel result validation[16] and prediction.[17]

RotCFD is built on multiple modules, allowing diversity in analysis problems. For the analyses performed in this paper RotUNS is utilised, this module is an unstructured flow solver capable of performing rotor-body interaction simulations, amongst others. RotUNS governing equations are unsteady, incompressible Reynolds Averaged Navier-Stockes equations using a $k-\epsilon$ turbulence model. This solver utilises a Cartesian unstructured grid in the farfield together with a body-fitted tetrahedral grid near the body.

RotUNS models the rotor as a distribution of momentum sources, this allows the rotor to be fitted with a Cartesian grid instead of requiring a body fitted grid. The momentum imparted by the rotor is dependent on geometry and flow characteristics of the rotor. These characteristics are defined in part through C81 database files describing the cross-sectional aerofoil at radial positions together with chord and twist curves along the radius of the blade. Cyclic, and flapping can also be included in the model whilst the radius, number of blades, cone angle, cutout radius, and hing offset effect the geometry. Finally setting collective and tip speed culminates in a full rotor model. The rotor can be modelled both as steady and unsteady, the steady case treating the rotor as a time-averaged source of momentum without taking into account instantaneous blade position.

As this software is under development results must be interpreted as an estimate, used to gauge the behavioural characteristics due to changes in test configuration and should not be taken as exact.

D. NDARC

NDARC[9,10] is an aircraft system analysis tool designed for conceptual design and technology impact assessments. Written for versatility and concept development the software is able to model advanced rotorcraft systems and analyse mission performance using models typically appropriate for the conceptual design environment quickly.

An NDARC job consists of one or more cases able to perform design or analysis tasks. A design task involves sizing of an aircraft to meet mission requirements whilst an analysis task can involve off-mission design performance, flight performance analysis, and general component performance mapping. For analysis tasks the design can come from a sizing task, from a previous NDARC job, or an independent design database. The culmination of this paper is an aircraft NDARC database were the geometry and aerodynamics stem from the analysis performed. The rotors and propulsion are taken from an existing XV-15 model.

The aircraft consists of a set of components, including rotors, wings, tail surfaces, and propulsion. For each component a set of attributes exist; such as performance, drag, weight, and geometry. Each of these attributes can be calculated or defined. Using different configurations of these basic components a variety of designs can be generated and analysed.

II. AVL analysis

The aircraft model is initially provided in an OpenVSP format. Using OpenVSP[5] this geometry is exported as a .hrm file. Here the geometry has been split into each component with cross-sections represented with a number of data points. The AVL analysis is only performed using the aircraft wings and therefore a python script is written to only export and build an AVL geometry file using the wing cross-sections. Each wing has three cross-sections with varying y locations for horizontal wings and varying z for vertical wings. No dihedral angles exist simplifying the data interpretation.

The exported wing profiles have only a small number of data points describing them; so a batch script is written utilising XFOIL and its capability of regenerating an aerofoil with a high number of data points. Since AVL does not account for profile drag in its model, analysis is performed with XFOIL estimating zero-lift drag coefficients as presented in *Table 1*. The XFOIL drag coefficients are normalised with dynamic pressure as the profile analysed is normalised to a length of unity.

With all wing profiles at each cross-section extracted the AVL geometry file is updated. This file includes each wing as a surface mirrored around the center line. Each wing is modelled with three cross-sections along it's span using a cosine vortex distribution. The intermediate wing sections are linearly interpolated by AVL, as the wings have a straight taper and sweep two cross-sections would suffice; but to correctly model the control surfaces a third is inserted. The control surfaces are highlighted in *Figure 1*, the surfaces in blue are omitted from the AVL model as they are used only in VTOL mode. *Figure 2* shows the final geometry used by AVL for the analysis.

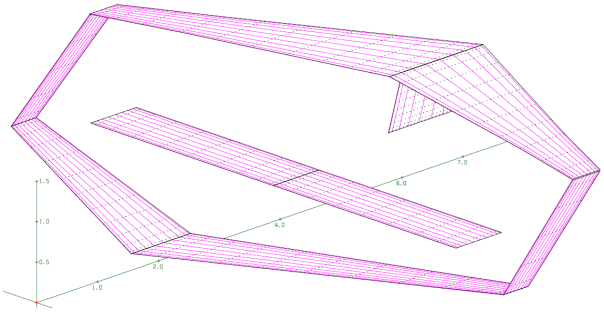

Figure 2: The AVL geometry of the aircraft used in analysis.

A. Limitations

AVL will only model lift induced drag, therefore the drag values represent only the change in drag due to lift. To make the analysis more representative, and avoid a zero drag at zero lift, the zero lift drag calculated with XFOIL is added; though XFOIL analyses only 2D aerofoils, it is deemed a good estimate for the zero-lift drag value. *Table 1* presents the zero-lift drag breakdown and the total drag coefficient added to the AVL drag results.

The fuselage is omitted from the AVL analysis as the streamlined body model that AVL implements is not expected to have a large impact on flow, but instead risks impairing the solver. Instead the wings are extended to the center-line. Though the fuselage is ommited from the AVL analysis it will still have a zero-lift drag that must be included in the drag estimation. Hoerner's streamlined body drag estimation[6] is used with the fuselage estimated to be a streamlined body with canopy and landing gear.

Table 1: Zero-lift drag coefficients calculated by XFOIL for wings and Hoerner's slender body drag estimate for the fuselage normalised to the total wetted area of wings.

Wing	C_{D0} Estimate	Reference area $[m^2]$	C_{D0}
Forward wing	0.0073	$2 \cdot 2.807/19.7$	0.0004
Center wing	0.0106	$2 \cdot 2.256/19.7$	0.0005
Aft wing	0.0055	$2 \cdot 3.863/19.7$	0.0003
Vertical stabiliser	0.0058	$2 \cdot 0.475/19.7$	0.0003
Vertical wings	0.0058	0.898/19.7	0.0003
Fuselage	0.0416	23.8/19.7	0.0503
Total zero lift drag	-	19.7	0.0577

Due to the design of the aircraft it is possible that angles of attack past a certain point will cause turbulent flow from the forward and center wings to disrupt flow over the aft wing and thereby compromise control authority. This phenomenon will possibly not be detected in AVL due to the nature of the solver. Therefore estimated control authority with this model may not be representative at higher angles of attack.

B. Forward flight out of ground effect

AVL can output a multitude of data, for this analysis strip forces, surface forces, and the total forces are saved. These results allow data required by NDARC to be calculated for each part as well as providing an estimate on the total aircraft performance. Flight cases are run at $57knots$, for angles of attack ranging between $-2°$ and $+16°$. As this requires a large

number of runs a batch script is utilised to automate the process. Results for higher angles of attack must be viewed with caution due to the limited stall evaluation.

The results of this analysis are presented together with the RotCFD results in *Figures 4 - 7*. For the NDARC database dynamics are not required, the data taken from AVL is simply aerodynamic characteristics for each lifting surface.

III. RotCFD analysis

The geometry model used in the RotCFD analysis differs slightly from that used in the AVL analysis. Instead of the OpenVSP model a CAD model of the actual prototype is provided that is converted into a water-tight .stl model. This model is split into it's different parts: forward wing, aft wing, center wing, vertical wings and stabiliser, and fuselage to allow a breakdown of where forces and moments are arising.

Also, in the RotCFD analysis rotors are used to estimate flow interactions between rotor wake and wings. As the proposed rotors do not have a final design a scaled XV-15 rotor model is used. The XV-15 is a tilt-rotor aircraft developed by Bell, in conjunction with NASA , in the 70's. It's rotors are designed with a compromise between hover performance and forward flight efficiency. Due to this rotor having been used and it's data available through analysis already performed[17] at the Aeromechanics branch at NASA Ames Research Center it is chosen as a good temporary model. As the XV-15 rotor is larger than the proposed rotor the model is scaled down to the proposed size, the proposed model is also planned as a five bladed rotor instead of three. With the rotor scaled down the RPM is increased to reach a similar tip speed.

A brief analysis is then performed with the rotor in RotCFD to estimate a required collective to achieve the design thrust of $4500N$ per rotor.

A. AVL comparison

For the AVL comparison the fuselage is omitted from the geometry and replaced by extending the wings to the center line. This is to gain a closer model to that used in the AVL analysis. The analysis is performed at $57knots$ for angles of attack ranging between $-2°$ to $+16°$.

The boundary box is set to a cuboid with width and height 20 times the aircraft wingspan and length 40 times the aircraft length. The aircraft is placed a distance equal to a quarter of the boundary length from the inlet. This size of test volume is deemed large enough for the walls not to interact with the aircraft. Closer to the model a refinement box is used to generate a high enough number of cells to provide sufficient flow resolution in the vicinity of the aircraft. Finally the body refinement is body-fitted and set high enough that the surfaces have acceptable resolution. The final grid is presented in *Figure 3* and is a compromise between result fidelity and computation time.

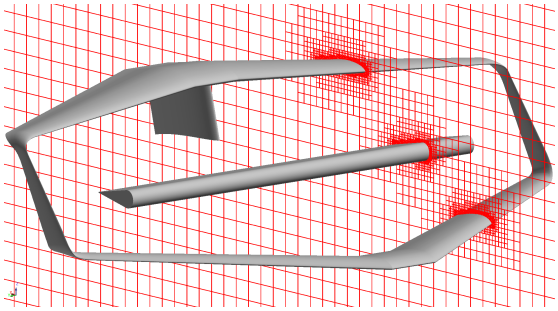

Figure 3: Grid and model used in AVL comparison analysis.

The boundary conditions are set to free flight and the flow properties set to standard atmosphere air at sea level.

Using (1) an appropriate time interval to run the simulation for is estimated so that a particle will pass by the whole model,

$$t = \frac{l_{test}}{V_{forward}}. \tag{1}$$

Ideally one would use a time interval that allows all particles present at the start of the analysis to exit the test area, this however is deemed too time consuming in the available time frame. A length of l_{test} is chosen for the particles to pass, a little longer than the model itself. With the time interval set, the number of steps in this interval must be calculated. A particle must not skip a cell during the analysis or risk effecting the results or diverging the solution completely. Therefore (2) is used to estimate the number of time steps required so that even the smallest estimated cell is not skipped,

$$n_s = \frac{n_{bc}}{\psi} \cdot (3 \cdot 2^{k-1} + 1). \tag{2}$$

Here n_s is the number of time steps required for the time it takes for the flow to pass n_{bc} boundary cells. n_{bc} is the number of boundary cells flow passes for a length of l_{test}. The smallest cell size is estimated with the expression to the right; k is the highest refinement level used with the $(3 \cdot 2^{k-1} + 1)$ originating from the nature of the tetrahedral grid, compared with (2^k) for a non-body fitted grid. ψ is the ratio between distance travelled and size of cell as shown in (3),

$$\psi = \frac{V \cdot \Delta t}{\Delta x}. \tag{3}$$

Δt is the time of one step and Δx the length of one cell. With constant V, $\psi \leq 1$ should hold to ensure no cells are missed by the flow. However due to the geometry being analysed ψ is chosen as 0.5, to account for velocity gradients and non-uniform tetrahedral cells.

The results of this analysis together with that of AVL are presented in *Figures 4 - 7*. An analysis including the fuselage is also presented in these figures, but still omitting the rotors.

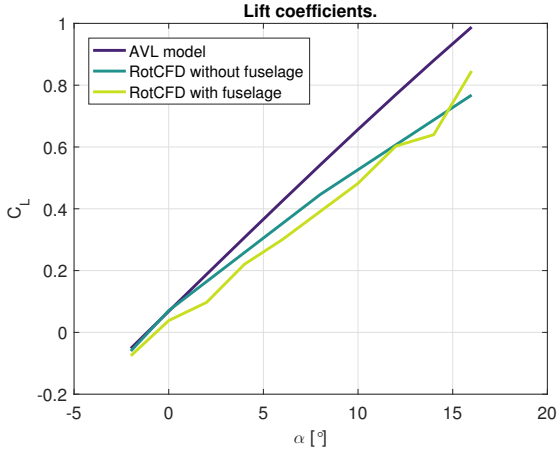

Figure 4: C_L curve.

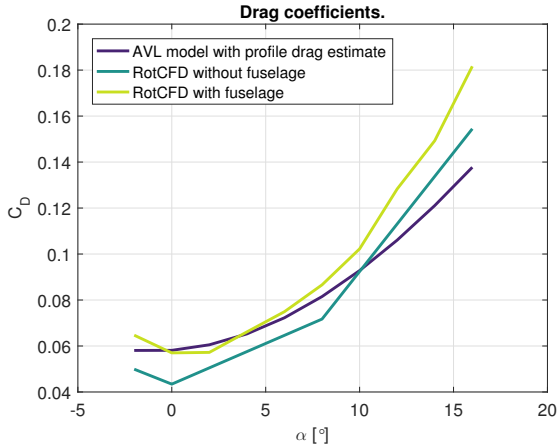

Figure 5: C_D curve.

The values correspond well for low angles of attack but deviate somewhat for larger angles.

B. Forward flight

Forward flight is now analysed including the rotors; the model is presented in *Figure 8* together with a grid slice. Unfortunately it is not possible to model control surfaces easily in RotCFD and so an analysis on control authority and turbulent interactions or

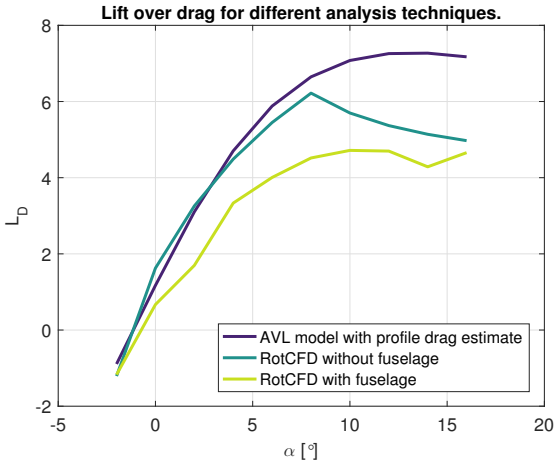

Figure 6: L/D curve.

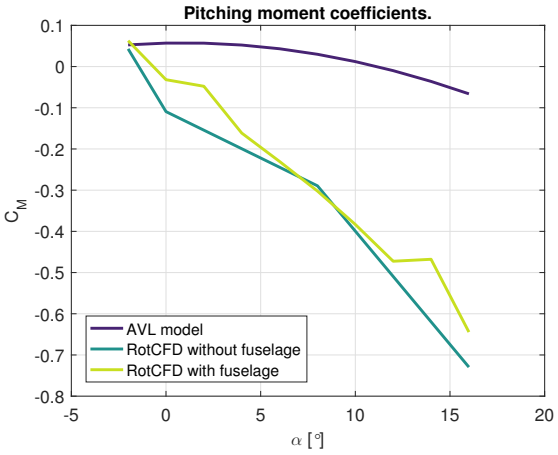

Figure 7: C_M curve.

wake effects on the aft wing and elevators can not be well estimated in the time frame. To begin the analysis only the forces and moments caused by aerodynamic effects are observed with a moment point on the center line $0.73m$ below the rotational axis of the center wing. These values are then used in a pitch stability estimation where rotor forces are also included.

1. *Body only forces and moments*

The analysis for forward flight is performed at $35kts$, $57kts$, and $70kts$. As this aircraft is a tilt-wing these analyses are performed for not only a range of angle of attack but also different tilt angles of the center wing. The same boundary conditions and sizing is used as in the AVL comparison and the refinement levels are kept the same.

Figures 10 - 11 presents the results of these analyses whilst *Figure 9* shows the flow interaction estimation made with RotCFD for the case with rotors at $57kts$ and zero tilt of the center wing.

From *Figure 9* it is clear that the rotor wake is

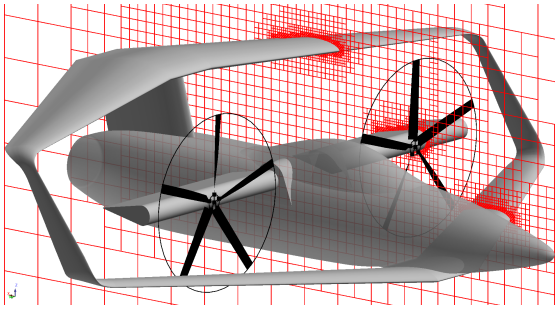

Figure 8: Model used in forward flight analysis together with a slice of the grid used.

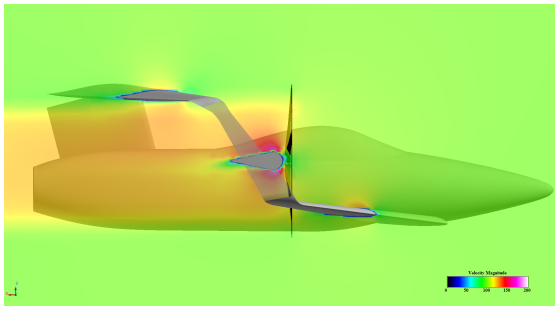

Figure 9: Visualisation of flow interaction between rotors and aft wing.

causing a higher velocity flow on the lower side of the aft wing than on the top, thus causing a negative lift and therefore a nose-up pitching moment. This is true for all cases run, though as the angle of attack is increased or the difference between rotor wake velocity and free-stream velocity decreases the negative lift contribution of the aft wing diminishes.

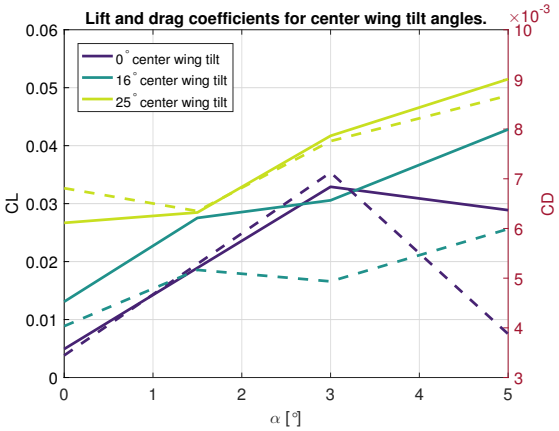

Figure 10: Lift and drag coefficients for a range of alpha with a number of tilt angles; here full line is C_L and dashed C_D.

As previously mentioned the results presented in *Figures 10 - 11* do not include contributions from the rotors themselves and are taken in a point $0.73m$ below the center wings rotational axis.

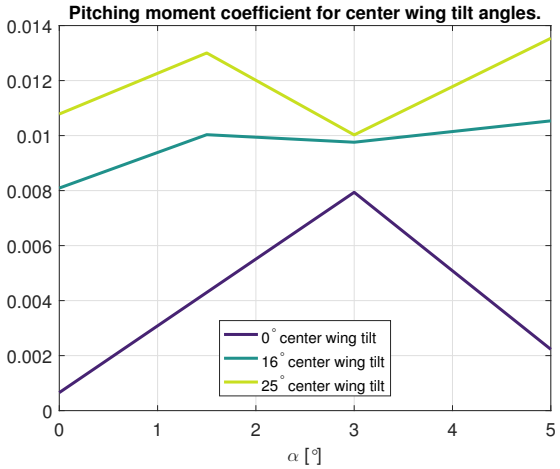

Figure 11: Pitching moment variation for alpha for a number of tilt angles.

2. *Pitch stability*

In this part of the analysis the center of gravity is assumed to be $0.73m$ below the center wing. This location is then varied in x to estimate the pitching moments sensitivity to movement of the center of gravity; *Figure 12* presents the range of locations used in this analysis.

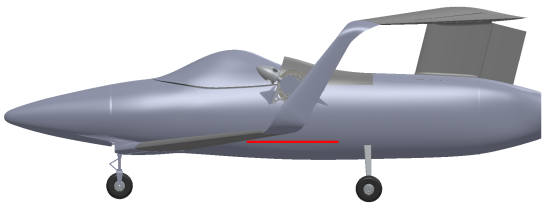

Figure 12: Line along which center of gravity location is varied in sensitivity analysis.

This analysis does not include control surfaces so these results are not static state. Yet a picture of the behaviour of the aircraft can still be imagined. *Figure 13* shows an example pitching moment contribution breakdown around a c.g. located $0.73m$ below the center wings rotational axis for a number of cases.

It is evident that as the angle of the tilt wing is increased the aft wing perturbs the aircraft's pitching moment, probably due to the rotor wake interaction; though *Figure 14* would suggest it is possible to place the c.g. to negate this nose-up pitching moment.

As the center of gravity moves forward of the center wing the pitching moment becomes smaller until it eventually becomes negative.

C. Hover

Hover is analysed out of ground effect as this is expected to require the most power. First the airframe

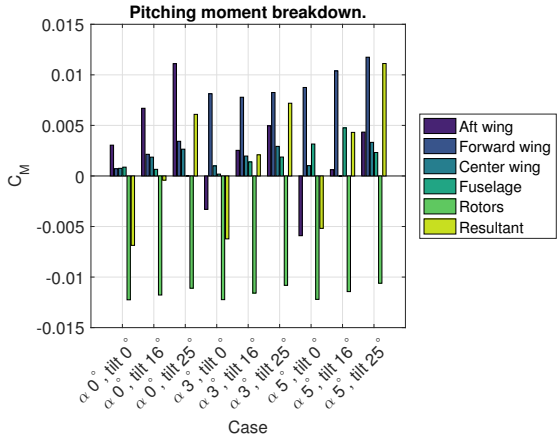

Figure 13: Pitching moment breakdown for a number of cases at $57kts$.

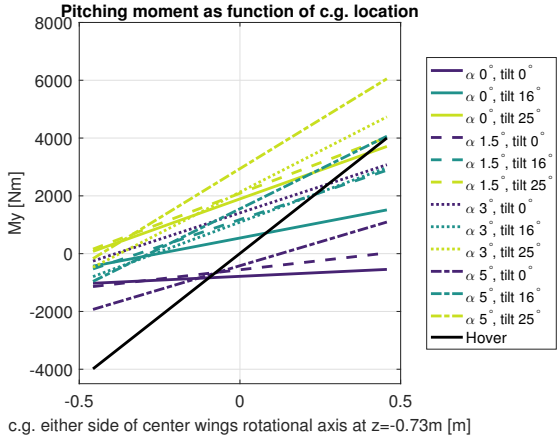

Figure 14: Sensitivity in pitch due to change in c.g. location at $57kts$ and hover.

is analysed with the rotor wake interactions. Results from the aerodynamic analysis are then used in a sensitivity analysis to changes in the center of gravity location.

1. *Aerodynamic analysis*

The tilt-wing and rotors are set to 90° incidence and the flight conditions set to hover in RotCFD. The boundary conditions are set to atmospheric pressure and no velocity.

The boundary box for this case is again modelled as a cuboid, this time with width and depth 40 times the rotor radius and height 80 times the rotor radius. In this analysis multiple refinement boxes are used to capture the wake propagation, one surrounding the whole aircraft to get a reasonable grid resolution in the vicinity of the aircraft and a second refinement box surrounding the rotors and center wing to capture the wake interaction.

For the hover case the time interval is decided from the estimated number of rotor rotations required to get a rotor wake propagated past the airframe. Using the estimated induced velocity and estimating a required propagation of 5 rotor radii a preliminary time interval is gauged with (4),[12]

$$t = \frac{5R}{\sqrt{\frac{T}{A}\frac{1}{2\rho}}}. \tag{4}$$

The result of this is rounded up to a time equal to a whole number of rotor rotations. With the time interval calculated it is again necessary to calculate the required time steps for a particle to not skip a cell. For the hover case this is driven by the rotor tip not skipping a cell as it's velocity is far greater than any other velocity in the flow, assuming the rotor grid has the same refinement level as the body. If the body and rotor have different refinement levels an estimation of required time steps must be performed for each and the maximum used, to avoid a cell being skipped. Equation (5) is used for the rotor case,

$$n_s = \frac{2^{k-1} \cdot \pi \cdot RPM \cdot R \cdot t \cdot l_{test}}{30 \cdot n_{bc}}, \tag{5}$$

where R is the radius of the rotor, k the refinement level of the rotor, and l_{test} the test section length corresponding to n_{bc} boundary cells. In hover the rotors are set to $2000RPM$ and generate roughly $4500N$ of thrust each. Due to the tilt-wing design limited download is expected, however a pitching moment is expected due to interaction with the forward wing. As can be seen in *Figure 15* this interaction is experienced.

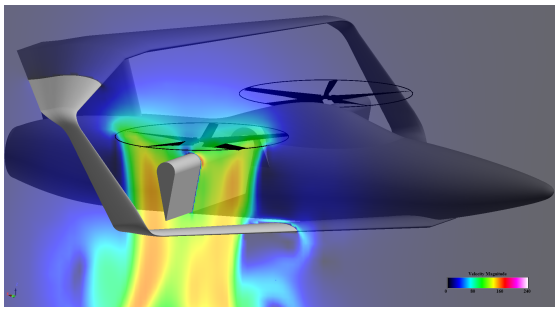

Figure 15: Flow interaction with wings in hover.

Figure 16 presents the flow field around the front wing; here it is visible that air flows around the forward wing. Assuming a fully propagated flow the forces and moments in hover are presented with the louver analysis results in *Figures 21 - 24*, see the ascent case.

In short the download is small enough that it should not impinge on hover ability. The pitching moment experienced is also small and should be controllable. However, as was performed in forward flight

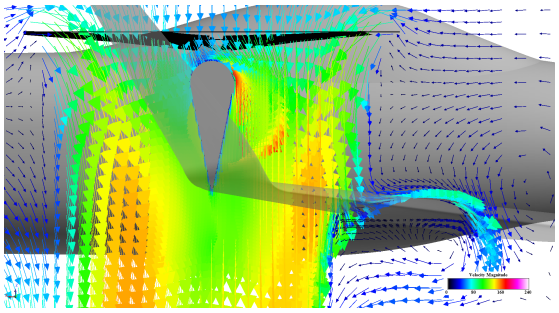

Figure 16: Flow around center wing and interaction with the forward wing.

analysis, a sensitivity analysis to a change in the center of gravity is performed.

2. Sensitivity to change in center of gravity location

As was done in the forward flight analysis the center of gravity is moved along the line shown in *Figure 12*. Included in this analysis are the forces generated by the rotors as well as the aerodynamic forces acting on the airframe. The impact this has on the moments experienced in hover is shown in *Figure 14*. The majority of forces experienced in hover originate from the rotors, due to this the aircraft is very sensitive to changes in the center of gravity's longitudinal location. If the center of gravity is placed in the location that gives zero pitching moment and having an interval of it's location of $1m$, $8kNm$ of torque is required from the tails pitch control to keep the aircraft steady.

IV. Louver analysis

The hover control of this aircraft does not utilise classic swash-plate, collective, and cyclic. Instead a louver design is used, these louvers are placed in the wake of the rotors with the aim of deflecting the downwash to create forces and moments. There are four different cases for the louvers: ascent, descent, roll, and yaw. Each case is analysed using a maximum louver deflection of 35°. The models used for each case can be found in *Figure 17*.

The boundary box and conditions used are the same as that for the hover case presented in the hover simulation. However in this analysis a third refinement box is included encompassing only the center wing. This is to better capture the flow interaction with the louver surfaces.

A. Ascent

The ascent model is the same as the model used in hover. Results from the hover case are presented in

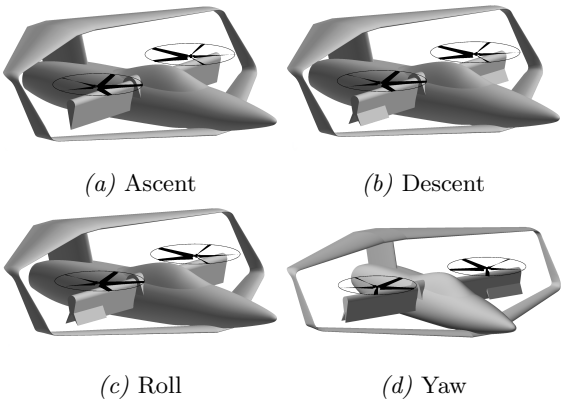

(a) Ascent *(b)* Descent

(c) Roll *(d)* Yaw

Figure 17: Models used for each louver case.

Figures 21 - 24 together with the three other louver configurations. The flow around the undeflected louver has been shown in *Figure 16*.

B. Descent

In the descent model the louver on each center wing deflects both it's surfaces fully. This is expected to increase download and in this way provide control of climb rate in hover. As the louvers are deflected symmetrically no rolling or yaw moment is expected, though due to the deflection of flow over the forward wing some change is expected in the pitching moment. *Figure 18* shows the deflected flow around the louver.

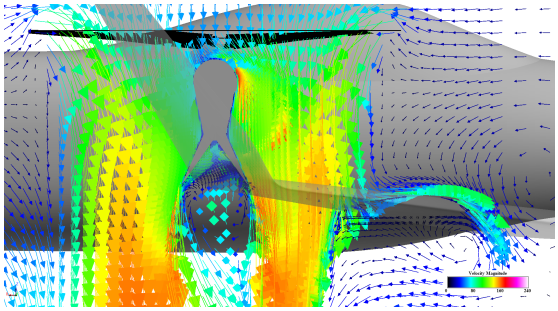

Figure 18: Flow around fully deflected louver.

C. Roll

Roll is achieved through a differential drag between each side of the aircraft. One louver fully deflects each surface, in this way generating more download. With the increase in download on one side of the aircraft a rolling moment will be experienced. Due to the asymmetry of this case coupling with yaw moment is expected and due to the deflection of flow over the forward wing some change in pitching moment from the ascent case is warranted. The difference in flow in the rotor wake can be seen in *Figure 19*.

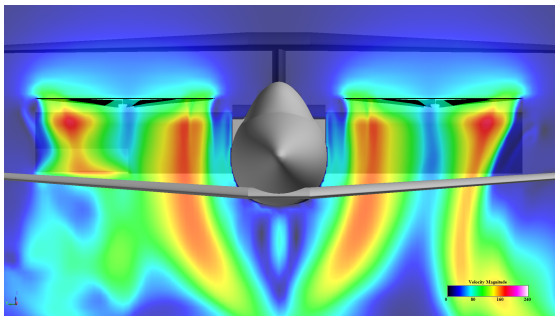

Figure 19: Difference in flow between fully deflected louver and undeflected louver giving a differential download.

D. Yaw

As with roll an asymmetric louver deflection is used to achieve yaw moment. In this case one opposing surface is deflected on each louver, generating differential lift on the center wing. This difference in lift on each side of the aircraft generates a yaw moment, however as the flow on one side of the aircraft is deflected over the forward wing not only will a yaw moment be experienced but also a pitching and rolling moment. In *Figure 20* the flow deflection caused by the louver is visible. It should also be noted that the rotational direction of the rotors causes differing loads on each louver causing unsymmetrical forces.

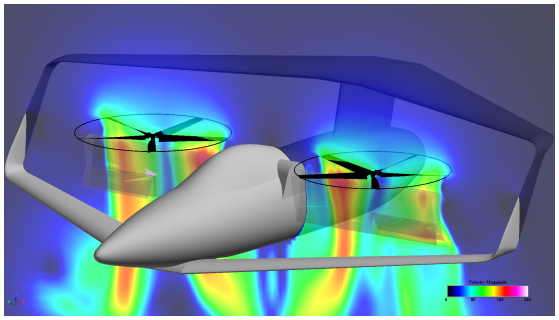

Figure 20: Flow difference due to asymmetric deflection of louver surfaces generating a yawing moment.

E. Results of louver analysis

The forces and moments resulting from the louver analysis are compiled here. Results are split into contributions from each component save the vertical surfaces, their contribution is close to zero for all cases and are therefore omitted. *Figure 21* presents lift and drag whilst the remaining plots, *Figures 22 - 24*, present the resulting moments in a point $0.73m$ below the rotational axis of the center wing. The rotors are not included in these values, though as they act through the moment point only lift should be impacted. Together the rotors generate $10300N$ of thrust giving a total lift force sufficient to hold the aircraft in hover.

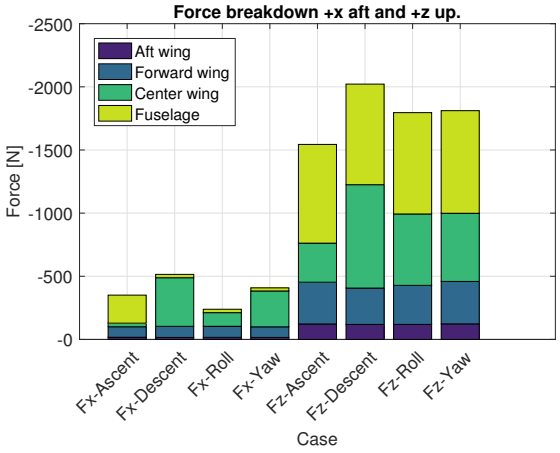

Figure 21: Lift and drag forces experienced for each louver case.

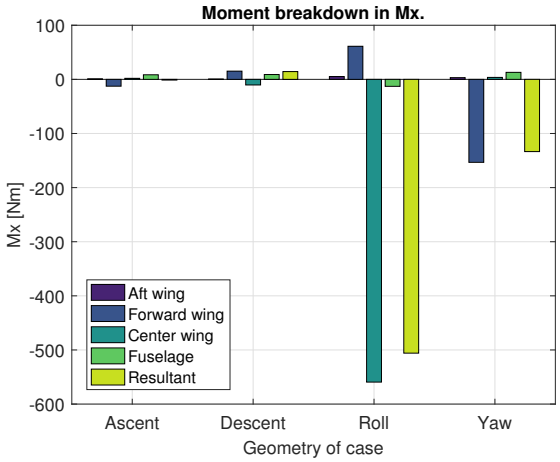

Figure 22: Moment experienced around x for each louver case.

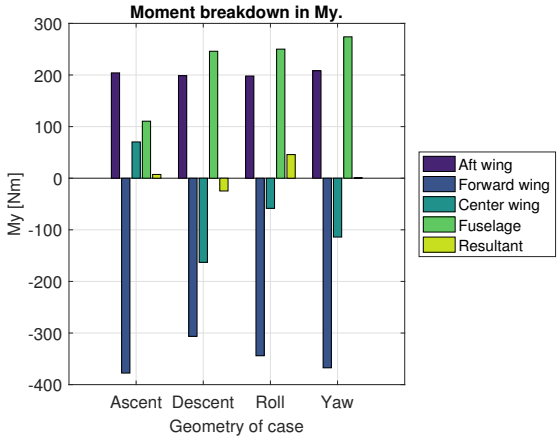

Figure 23: Moment experienced around y for each louver case.

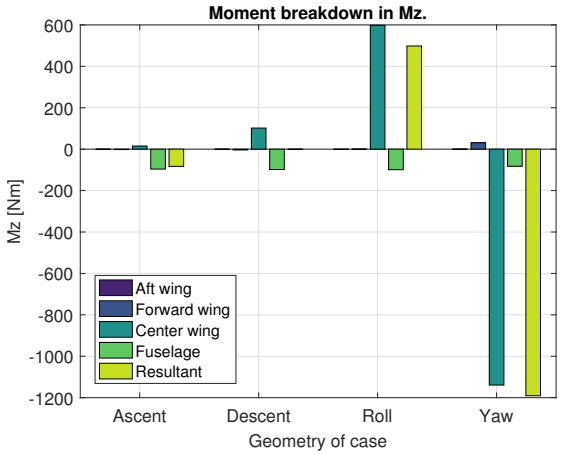

Figure 24: Moment around experienced z for each louver case.

V. Summery

As the results have been presented throughout the paper a brief discussion will be held summarising the results and their possible impacts. First the NDARC database is briefly presented before moving onto a general discussion of the analysis and tools used.

1. *NDARC*

The analysis performed enables the generation of an NDARC database describing the Elytron 2S aircraft. The aircraft is modelled as a fuselage, two wings and five tails, two rotors, and a propulsion group. The wings represent the forward wing and the center tilt-wing. The tails are modelled to represent the aft wing, vertical wings, and the vertical stabiliser. The rotors are mounted to the center wing and their incidence linked.

With the components defined their locations are set to represent the Elytron 2S configuration. The resulting aircraft geometry is represented by the sketch generated by NDARC found in *Figure 25*. This is a simple means to check the geometry is defined correctly visually; however there are an assortment of output files available to confirm proper interpretation of inputs. As NDARC is designed to be versatile it is easy to miss definition flags, therefore proper checking of the internal configuration used in the analysis is essential.

This database file allows further aircraft analysis to be performed. Trim and performance analysis can be performed in NDARC allowing dynamics to be modeled with the newly developed tool SIMPLI-FLYD[11]
.

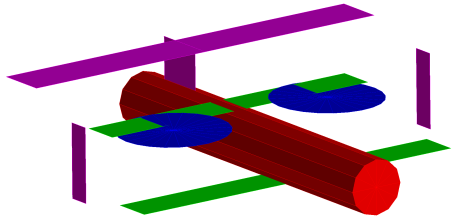

Figure 25: NDARC sketch.

2. *Discussion*

In short the airframe seems stable in it's self, however with the introduction of rotor wake interaction effects are experienced. It would seem possible to attain a stable configuration in forward flight with careful placement of the center of gravity.

AVL and RotCFD lift and drag results correlate well for small angles of attack for the bare airframe. However AVL is vastly quicker than RotCFD. It is also easy to extract data, either for full aircraft forces and moments or individual surfaces forces and moments. For small angle of attacks, simple configurations, and no rotors AVL is a good tool for fast aerodynamic characterisation.

With the inclusion of the rotors AVL is no longer a software that can be used; in these cases RotCFD is a CFD tool with good solution times. Being able to use simple rotor models generation of RotCFD cases is less time consuming and focus can be put on running as many relevant cases as possible. As the steady rotor model is used to save time fluctuating pressures are not taking into account. Despite some cases requiring tuning of the time grids to find convergence, overall the analysis tool is very easy to use. The flow results generated with RotCFD show rotor wake interaction with the wings and the forces resulting from this are present in the output. Due to the symmetrical nature of the geometry and analysis performed, forward flight side forces arising are interpreted as noise from the solver. Some cases converge to seemingly wrong values outside this noise; it must be remembered that this code is in development and so results used with some caution.

Through the pitch sensitivity analysis it is possible to see that the forward flight and hover center of gravity requirements do not correlate well. This may mean that it will be challenging to make the transition between hover mode and forward flight smoothly. Though if VTOL capabilities are sidelined for the moment it does seem possible to find a stable configuration. Again, as control surfaces have not been modelled in RotCFD, it is difficult to know the magnitude of control authority variation due to the rotor wake.

VI. Conclusion

To conclude this paper it is anticipated that a stable configuration of the aircraft exists. The airframe performs well in forward flight in the vicinity of $57kts$. It should, with well designed propellers, also be able to hover. Issues may arise during the transition between hover and aircraft mode, however with good preparation and detailed analysis stable flight should be possible.

The software used to perform the analysis has been easy to use and generate consistent results. They have proven themselves adept at allowing quick analysis and characterisation of aircraft in early stages of design and testing as well as being easy to use and grasp.

I look forward to following the progress of the flight testing of the aircraft and hope to see it flying in coming years.

Acknowledgments

There are a multitude of acknowledgements to be made, starting with Dr. William Warmbrodt* for offering me this project and his support throughout it. This opportunity stems from the resent cooperation of the Swedish National Space Board (SNSB) together with the education office at NASA Ames Research Center. Without the cooperation of these two organisations this opportunity and experience would not have been made available to me.

The second cooperation enabling this research is that of Elytron and NASA, lead by Dr. Colin Theodore† on NASA's side. Dr. Theodore also supervised my work together with Dr. Ben Lawrence† who provided invaluable guidance.

For assistance getting started with RotCFD and how best to utilise it I would like to thank Eduardo Solis†, Natasha Barbely†, and Dr. Ganesh Rajagopanal‡.

I must thank Adam Ewert§ and Eduardo Solis† for generating the models used in the RotCFD analysis.

My gratitude goes out to Dr. Wayne Johnson† for assistance with debugging of the NDARC model.

For support throughout this internship I thank my family and girlfriend, as well as her family.

Finally I thank the Spring 2016 interns for all the laughs and experiences we have enjoyed together, as well as everyone at NASA Ames and the aeromechanics department for making me feel right at home.

*Cheif of the Aeromechancis department at NASA Ames Research Center

†Aeromechanics department at NASA Ames Research Center.

‡Sukra Helitek Inc.

§Aerospace undergraduate at New Mexico State University.

References

[1]Elytron, *Online*, Available at: `http://elytron.aero/`, Last accessed 21/04/16.

[2]Drela, M., Youngren, H., *Online*, [Updated 29 Jan 2015], Available at: `http://web.mit.edu/drela/Public/web/avl/`, Last accessed 21/04/16.

[3]Drela, M., Youngren, H., *Online*, [Updated 23 December 2013], Available at: `http://web.mit.edu/drela/Public/web/xfoil/`, Last accessed 21/04/16.

[4]Sukra Helitek Inc., *Online*, Available at: `http://sukra-helitek.com/rotcfd.html`, Last accessed 21/04/16.

[5]OpenVSP, *Online*, Available at: `http://www.openvsp.org/`, Last accessed 21/04/16.

[6]Hoerner, S.F., "Fluid-Dynamic Drag", Published by the Author, 1965, Chap VI and Chap XIII.

[7]Johnson, W., "NDARC-NASA Design and Analysis of Rotorcraft Theoretical Basis and Architecture", Presented at the *American Helicopter Society Specialists' Conference on Aeromechanics,* January 20-22, 2010.

[8]Johnson, W., "NDARC-NASA Design and Analysis of Rotorcraft Validation and Demonstration", Presented at the *American Helicopter Society Specialists' Conference on Aeromechanics,* January 20-22, 2010.

[9]Johnson, W., "NDARC NASA Design and Analysis of Rotorcraft", NASA/TP-2015-218751

[10]Johnson, W., "NDARC NASA Design and Analysis of Rotorcraft Theory Appendix 7", NASA/TP-2009-215402, December, 2012.

[11]Lawrence, B., Tobias, E.L., Theodore, C., Berger, T., Tischler, M.B., Elmore, J., "Integrating Flight Dynamics & Control Analysis and Simulation in Rotorcraft Conceptual Design", To be presented at *AHS 72nd Annual Forum*, West Palm Beach, FL, May 17-19, 2016.

[12]Leishman, J.G., "Principles of Helicopter Aerodynamics", Second Edition, Cambridge University Press, 2006, Chapter 2.

[13]Rajagopalan, R.G., Baskaran, V., Hollingsworth, A., Lestari, A. Garrick, D., Solis, E., Hagerty, B., "RotCFD - A Tool for Aerodynamic Interference of Rotors: Validation and Capabilities", *AHS Future Vertical Lift Aircraft Design Conference*, January 18-20, 2012 San Francisco.

[14]Guntupalli, K., Novak, L.A., Rajagopalan, R.G., "RotCFD: An Intergrated Design Environment for Rotorcraft", Presented at the *AHS Specialists' Conference on Aeromechanics Design for Vertical Lift*, San Francisco, California, January 20-22, 2016.

[15]Barbely, N.L., Komerath, N.M., Novak, L.A., "A study of Coaxial Rotor Performance and Flow Field Characteristics", Presented at the *AHS Technical Meeting on Aeromechanics Design for Vertical Lift*, Fisherman's Wharf, San Francisco, CA January, 20-22, 2016.

[16]Sahin, S.E., Russell, C.R., Solis, E., Rajagopalan, R.G., "Analysis of Large Civil Tilt Rotor Wind Tunnel Blockage and Validation Using RotCFD", Presented at the *AHS International Technical Meeting on Aermechanics Design for Vertical Lift*, San Francisco, California, January 20-22, 2016.

[17]Koning, W., Acree, C.W., Rajagopalan, R.G., "XV-15 Tilt Rotor Performance Validation Using Computational Fluid Dynamics", *AHS Technical Meeting on Aeromechanics Design for Vertical Lift*, Holiday Inn at Fisherman's Wharf, San Francisco, CA, January 20-22, 2016.

[18]Pereira, R.L., "Validation of software for the calculation of aerodynamic coefficients with a focus on the software package Tornado", *Degree Project*, Linkping University, Department of Management and Engineering, Fluid and Mechanical Engineering Systems, 2010.